JOURNAL OF AIRCRAFT
Vol. 41, No. 3, May–June 2004

Identification of Computational-Fluid-Dynamics Based Unsteady Aerodynamic Models for Aeroelastic Analysis

Daniella E. Raveh*
Technion—Israel Institute of Technology, 32000 Haifa, Israel

Three approaches for reduced-order modeling of computational-fluid-dynamics-(CFD) based unsteady aerodynamics, employing system-identification methods, are presented, and used for generation of three models: A frequency-domain model, a time-domain autoregressive-moving-average model, and a discrete-time state-space model. All models are identified based on the same identification data, which consists of the time histories of the generalized aerodynamic forces developed in response to filtered white-Gaussian-noise modal excitation, computed in a CFD analysis. The models are used for rapid flutter analysis via traditional frequency-domain methods, linear stability analysis, and time simulation. The method is applied for flutter analysis of the AGARD 445.6 wing. The filtered white-Gaussian-noise input is found to be applicable within the framework of CFD, yielding informative identification data sets. The identification process is simple, and the resulting reduced-order models closely reproduce the CFD system response to various excitations. Reduced-order model-based flutter analysis is rapid and yields accurate results compared with wind-tunnel test, CFD, and linear aerodynamics results.

Introduction

IT is widely recognized that computational-fluid-dynamics (CFD) methods hold significant advantages over linear panel methods in their ability to accurately predict the nonlinear flowfields in the transonic flow regime. Yet, in spite of CFD advantages, the currently most-used unsteady aerodynamic method for aeroelastic applications is the linear doublet-lattice method.[1] A nonlinear aeroelastic simulation can be carried out by direct coupling of the CFD and the elastic structure equations and can be used for prediction of transonic aeroelastic instabilities. However, such use of CFD-based aeroelastic simulations is limited because of the typically large run times associated with each simulation, and because aeroelastic instabilities can only be predicted by performing many such simulations, studying each transient for decaying or diverging responses.

Recently, significant research is carried out in the development of reduced-order models (ROM). ROMs are simple models of the system that capture, to some extent, the nonlinear flow characteristics and are significantly more computationally efficient than the full CFD simulation. Characteristically, the "system" for which a ROM is sought is the aerodynamic system whose outputs are the unsteady aerodynamic forces that develop in response to structural elastic motions (the input). The aerodynamic ROM can be coupled with the structural model for aeroelastic analysis, either by replacing the full CFD solution in a time-marching simulation, or in stability analysis. Reviews of current reduced-order modeling approaches can be found in Refs. 2–4.

Linearized ROMs are very widespread among existing approaches, as they can be used directly with common linear flutter analysis tools. Linearized reduced-order modeling approaches rely on linearization of the nonlinear unsteady aerodynamic flow equations, assuming that the amplitude of the unsteady motion is limited to small perturbations about the nonlinear steady-state flow condition. Although linearized, these ROMs have considerable advantage over linear models, as they retain the nonlinear features of the main flow about which they are generated. These linearized models can be used in aeroelastic simulations, in stability analyses to predict flutter boundaries or in aeroservoelastic analyses. Linearized ROM can offer major improvement to the current practice of aeroelastic and aeroservoelastic analyses, provided that they can be derived in a practical manner that is applicable to the analysis of realistic aircraft configurations.

Various approaches to linearized ROMs can be found in the literature. Examples are the use of indicial responses by Ballhaus and Goorjian,[5] the pulse transfer-function analysis by Lee-Rausch and Batina,[6] and the use of the Volterra theory as proposed by Silva,[7] retaining only the first linear kernel by Raveh et al.[8] The just-mentioned approaches result in frequency-domain ROMs. Direct identification of discrete time-domain models was proposed by Cowan et al.[9,10] [an auto regressive-moving-average (ARMA) model identified from CFD response to a 3211 signal] and recently by Silva and Bartels[11] (a state-space model from CFD impulse responses).

The current study considers several methods for ROM identification, which result in three types of models: 1) a frequency-domain model, 2) a discrete time-domain ARMA model, and 3) a discrete time-domain state-space model. The identification of all models uses the same identification data, which consists of the time histories of generalized aerodynamic forces developed in response to a white-Gaussian-noise modal excitation, computed in a CFD run.

The method is applied to the AGARD 445.6 wing, a standard test case for transonic unsteady aerodynamic methods.[12] The aerodynamic ROMs are coupled with the structural model, and flutter boundaries are determined, using frequency and time-domain methods. Flutter results are compared to those from wind-tunnel tests and to flutter results based on linear aerodynamics. The accuracy and ease of implementation of the various models are evaluated and discussed.

Methodology

Reduced-Order Modeling

The aeroelastic CFD system, which consists of the flow equations and boundary conditions, is regarded as a dynamical system. The system's inputs are the modal motions of the structure, which are prescribed as time-dependent boundary conditions, and the outputs are the generalized unsteady aerodynamic forces (GAFs) that develop in response to the modal motions. For small-amplitude modal motions, the CFD system's response is linear, and linearized ROMs are identified.

The identification data consist of modal input–output time histories. The assumption of linearity implies that the response to a certain modal motion is independent of other modal motions. Thus

Presented as Paper 2003-1407 at the Structures, Structural Dynamics and Materials, Norfolk, VA, 7–10 April 2003; received 16 June 2003; revision received 10 September 2003; accepted for publication 10 September 2003.

*Senior Lecturer, Faculty of Aerospace Engineering. Member AIAA.

it is possible to excite the modes one at a time and either 1) identify a separate ROM for the response to each mode, in which case the system's response to an input that is a combination of modes can be obtained as a superposition of responses; or 2) concatenate the data sets to obtain a data set of responses to all modes, and identify one multiple-input/multiple-output (MIMO) ROM.

Three identification methods are described next; 1) identification of a frequency-domain model, 2) identification of a discrete time-domain ARMA model, and, 3) identification of a discrete time-domain state-space model.

Frequency-Domain ROM

The aeroelastic equation of motion in generalized coordinates is stated as

$$GM\ddot{\xi} + GK\xi - qF_A(t) = 0 \tag{1}$$

where GM and GK are the generalized mass and stiffness matrices, respectively, and $\boldsymbol{F}_A$ is the vector of generalized aerodynamic forces normalized by the dynamic pressure q. The generalized aerodynamic forces are dependent on the structural deformations, their time histories, and on the time histories of the generalized aerodynamic forces themselves. Traditional frequency-domain flutter methods are based on the assumption that, at the flutter point, the modal motions are simple harmonic motions, so that Eq. (1) can be written as

$$\left[-\omega_f^2 GM + GK - q_f GAF(k)\right]\xi = 0 \tag{2}$$

where k is the reduced frequency defined as $k = \omega b/U$, ω is the physical frequency, and b and U are the reference semichord and velocity, respectively. $GAF(k)$ is the matrix of complex generalized aerodynamic force coefficients, in which the ith column represents the generalized forces in all modes caused by a unit-amplitude harmonic motion of the ith mode. Frequency-domain GAF models consist of the complex GAF matrices at distinct values of reduced frequencies. They can be used in Eq. (2), in frequency-domain flutter analyses, such as the k, p–k, and g methods (see Chap. 7 of Ref. 13).

Based on some identification data, frequency-domain GAF models can be identified from either Fourier or spectral analysis. Lee-Rausch and Batina[6] applied a Fourier analysis to estimate the GAF frequency response from a data set containing the CFD system's response to a smoothly varying exponentially shaped input signal. The GAF frequency response was obtained by taking the Fourier transform of the output signal divided by the Fourier transform of the input signal.

A drawback of the preceding approach (Fourier analysis) is that the frequency response is not necessarily a smooth function of the frequency. This is because this type of modeling does not impose any model structure and does not assume anything about the system (except for its linearity). In fact, as shown in the Results section, the frequency response can be erratic, depending on the input signal. A smooth frequency response is obtained by means of spectral analysis, as follows. The frequency response is calculated by taking the estimated cross spectral density of the input and output signals $P_{\xi F_A}(k)$, divided by the power spectral density (PSD) of the input signal $P_{\xi\xi}(k)$, according to:

$$GAF(k) = \frac{P_{\xi F_A}(k)}{P_{\xi\xi}(k)} \tag{3}$$

where improved estimates of the spectral densities $P_{\xi\xi}(k)$ and $P_{\xi F_A}(k)$ are obtained by Welch's averaged modified periodogram method.[14] In Welch's method, the signals are divided into segments and "windowed" by a weighting function. Discrete Fourier transform (DFT) is performed on each segment, and the magnitude of the DFT is squared to provide the segment's PSD. The PSDs of the segments are averaged to provide the modified, smoothed PSD of the signal. This method is implemented in MATLAB's® Signal Processing Toolbox.[15]

The resulting GAF is a smooth function of the frequency, specified at distinct k values. Using the preceding approach, the GAF matrices can be evaluated at many reduced frequency values, with very little computational cost. This is an important feature for flutter analysis, in which interpolation between various reduced frequencies is typically necessary.

Time-Domain ARMA Model

The GAF ARMA model relates the generalized aerodynamic forces to the modal displacements at the current and previous time steps and to previous time-step values of the generalized forces. For a single mode case (single input single output), it assumes the following model structure:

$$\begin{aligned} F_A(n) = &-a_1F_A(n-1) - a_2F_A(n-2) - \cdots - a_{n_a}F_A(n-n_a) \\ &+ b_0\xi(n) + b_1\xi(n-1) + \cdots + b_{n_b}\xi(n-n_b) \end{aligned} \tag{4}$$

where ξ and $\boldsymbol{F}_A$ are the generalized modal displacements and the generalized aerodynamic forces normalized by the dynamic pressure, n is the discrete time variable, n_a and n_b are the model orders that are determined by the user, and $a_1 \cdots a_{n_a}$, b_0, $b_1 \cdots b_{n_b}$ are the model parameters to be estimated.

From Eq. (4), the predicted output $\hat{F}_A$ can be posed as

$$\hat{F}_A = H^T(n)\hat{\theta} \tag{5}$$

where H is the regression vector:

$$\begin{aligned} H = [&-F_A(n-1) - F_A(n-2) \cdots - F_A(n-n_a)\xi(n)\xi(n-1) \\ &\cdots \xi(n-n_b)]^T \end{aligned} \tag{6}$$

and

$$\hat{\theta}^T = \begin{bmatrix} a_1 & a_2 & \cdots & a_{n_a} & b_0 & b_1 & \cdots & b_{n_b} \end{bmatrix} \tag{7}$$

and the prediction error $\tilde{F}_A$ is defined as

$$\tilde{F}_A = F_A - \hat{F}_A = F_A - H^T(n)\hat{\theta} \tag{8}$$

where F_A is the measured output. The parameters that minimize the prediction error of Eq. (8) in a least-square sense are given by (see Chap. 7.3, pp. 203–211 of Ref. 16):

$$\hat{\theta} = \arg\min\left\{\frac{1}{N}\sum_{n=1}^{N}\tilde{F}_A^2\right\} = (H^TH)^{-1}H^TF_A \tag{9}$$

where N is the training data length.

For the MIMO case, Eq. (4) becomes

$$\begin{aligned} \{F_A(n)\} = &-[a_1]\{F_A(n-1)\} - [a_2]\{F_A(n-2)\} - \cdots - [a_{n_a}] \\ &\times \{F_A(n-n_a)\} + [b_0]\{\xi(n)\} + [b_1]\{\xi(n-1)\} \\ &+ \cdots + \left[b_{n_b}\right]\{\xi(n-n_b)\} \end{aligned} \tag{10}$$

where the i, j element of matrix $[a_k]$, $k = 1 \ldots na$ relates the output of the ith mode to the output of the jth mode at time $(n-k)$; and the i, j element of matrix $[b_k]$, $k = 0 \ldots nb$ relates the output of the ith mode to the input of the jth mode at time $(n-k)$. In this study it is assumed that the ith mode generalized force is dependent on past values of the ith generalized force only, thus making matrices $[a_k]$, $k = 1 \ldots na$ diagonal. In the MIMO case the least-square estimate minimizes the norm of $\tilde{F}_A^T\tilde{F}_A$.

Because the identification of model parameters from Eq. (9) is quick, several model orders can be tested to arrive at the best model order. The ARMA model of Eq. (4) can be used with a discrete-time version of the aeroelastic equation [Eq. (1)] for rapid aeroelastic simulations at various values of dynamic pressures.

Discrete-Time State-Space Models

The state-space discrete-time model of the aerodynamic forces assumes the following model structure:

$$x_A(n+1) = A_A x_A(n) + B_A \xi(n)$$

$$F_A(n) = C_A x_A(n) + D_A \xi(n) \tag{11}$$

The matrices A_A, B_A, C_A, and D_A can be estimated by using subspace methods based on least-squares techniques (see Chap. 7.3, pp. 203–211 of Ref. 16), as implemented in the MATLAB's System Identification toolbox.[17] Alternatively, a state-space aerodynamic model could also be specified based on the ARMA model, as proposed in Ref. 10. In that case, the states have a physical significance, that is, they are the previous-time aerodynamic forces and generalized displacements.

Time-Domain Flutter Analysis

The structure equation of motion, Eq. (1), can be written in state-space form as

$$\dot{x}_S(t) = A_S x_S(t) + q B_S F_A(t)$$

$$\xi(t) = C_S x_S(t) + q D_S F_A(t) \tag{12}$$

where

$$x_S(t) = \begin{Bmatrix} \xi \\ \dot{\xi} \end{Bmatrix} \tag{13a}$$

$$A_S = \begin{bmatrix} 0 & I \\ -GM^{-1}GK & 0 \end{bmatrix}, \qquad B_S = \begin{bmatrix} 0 \\ GM^{-1} \end{bmatrix} \tag{13b}$$

$$C_S = [I \quad 0], \qquad D_S = [0] \tag{13c}$$

and in discrete-time state-space form as[18]

$$x_S(n+1) = \bar{A}_S x_S(n) + q \bar{B}_S F_A(n)$$

$$\xi(n) = C_S x_S(n) \tag{14}$$

where

$$\bar{A}_S = e^{A_S T}, \qquad \bar{B}_S = \int_0^T e^{A_S \tau}\, \mathrm{d}\tau\, B_S \tag{15}$$

Equation (14) is coupled with the aerodynamic discrete state-space model, Eq. (11), to yield the coupled aeroelastic system equation:

$$\begin{Bmatrix} x_S(n+1) \\ x_A(n+1) \end{Bmatrix} = \begin{bmatrix} \bar{A}_S + q\bar{B}_S D_A C_S & q\bar{B}_S C_A \\ B_A C_S & A_A \end{bmatrix} \begin{Bmatrix} x_S(n) \\ x_A(n) \end{Bmatrix}$$

$$\xi(n) = [C_S \quad 0] \begin{Bmatrix} x_S(n) \\ x_A(n) \end{Bmatrix} \tag{16}$$

Linear stability analysis can be applied to compute the flutter characteristics of the aeroelastic system of Eq. (16).

Excitation Signal

Two types of input signals are implemented in this study. The basic signal is a numerically generated random time series (will be referred to as random), and the second signal is a filtered random time series with Gaussian distribution (will be referred to as filtered white Gaussian noise, or FWGN). In the latter, filtering is applied to control the range of excited frequencies, such that any frequency spectrum of interest can be excited. The basic random signal is generated in the CFD code, during the run, while the FWGN is generated offline, in MATLAB, and read as an input to the CFD run. Both signals are limited to small amplitudes. It will be shown in the numerical example section that both signals are applicable within the framework of CFD and provide adequate identification data.

Once the input signal is selected, a key objective is to determine the sampling rate and the required length of the data, such that all signals within the frequency range of interest are well characterized. Because the excitation is applied to the CFD system, which by itself is a discrete-time system, the intervals at which the excitation is applied and the system is sampled, correspond to the CFD time step Δt. The sampling rate is therefore $f_s = 1/\Delta t$, from which signals of frequencies of up to half the sampling rate, denoted by f_{Nyq}, can be reconstructed (based on the Nyquist Theorem, see Chap. 13.7, pp. 444 and 445 of Ref. 16). Because in CFD analyses the typical time steps are very small, the maximum frequency that can be identified is high and exceeds the typical frequency range of interest for aeroelastic problems.

The frequency resolution of a length-N data set, given by f_{Nyq}/N, should be adequate for the representation of the lowest frequencies of interest of the aeroelastic problem. Therefore, the sampling interval and the length of the sampled signal (the number of samples) need to be adjusted to fit the desired frequency range and resolution.

In the current application, the CFD time step was set to $\Delta t = 0.05$ nondimensional seconds (nd-s), based on stability limits of the CFD scheme. This is the largest possible time step for the numerical scheme and the specific test case. From this sampling interval, nondimensional frequencies of up to $f_{\mathrm{Nyq}} = 10$(cyc/nd-s) can be reconstructed. A nondimensional frequency of 10(cyc/nd-s) corresponds to a dimensional frequency of 11164 Hz (computed by $f_{\mathrm{nd}} = f \times L_{\mathrm{ref}}/a_{\mathrm{inf}}$ using the reference sea-level speed of sound $a_{\mathrm{inf}} = 1116.4$ ft/s and a reference length of $L_{\mathrm{ref}} = 1$ ft). For the AGARD 445.6 wing, the frequency range of interest is bounded by the fourth and highest structural mode at $f = 91.5$ Hz; thus, it is clear that this sampling rate is sufficiently small, and it can be assumed that all of the frequencies of interest are well represented in the data.

The CFD response was recorded over as many as $N = 2^{13}$ time steps, providing a frequency resolution of 0.0012 cyc/nd-s, or 0.7Hz. This length of the response is relatively large and requires significant computational time. It will be shown in the numerical example that while the frequency-domain models require large data sets, in the order of 2^{11} samples, for accurate identification of the low-frequency range, time-domain models require much shorter data sets, as short as 2^7 to 2^9 points, for accurate model identification.

Numerical Test Case

The proposed ROM methodology of this study is demonstrated with the AGARD 445.6 wing. The AGARD 445.6 wing was tested for flutter characteristics in the Transonic Dynamic Tunnel at NASA Langley Research Center[12] and was used as a test case in many studies of transonic aerodynamics.[6,8,9]

The flow is analyzed using the in-house Elastic Zonal Navier–Stokes Simulation (EZNSS) code.[19] EZNSS is a time-accurate implicit finite-difference code, based on the Beam and Warming algorithm, which is capable of analyzing the static and dynamic flowfields over a maneuvering elastic vehicle.[20] The problem setup is described in detail in Ref. 8. The CFD mesh is one of typical size for the problem at hand (wing only) and the CFD method (Euler). Initial analysis provided the steady-state inviscid flow field at several Mach numbers, at a zero angle of attack. In the lack of wind-tunnel pressure measurements for the AGARD 445.6 wing, comparison to results obtained with other codes served as a verification of the EZNSS results.[8] It is within the philosophy of the current study approach to demonstrate that a typical grid can serve for the identification process, and there is no need for a special, dense grid for this task.

The structural modal model of the wing consists of four elastic modes that can be characterized as first bending, first torsion, second bending, and second torsion.[8,12] An EZNSS time-stepping analysis provided the time histories of the GAFs in all four modes that developed in response to excitation of each mode. These responses served as the identification data sets, from which the various GAF ROMs were generated.

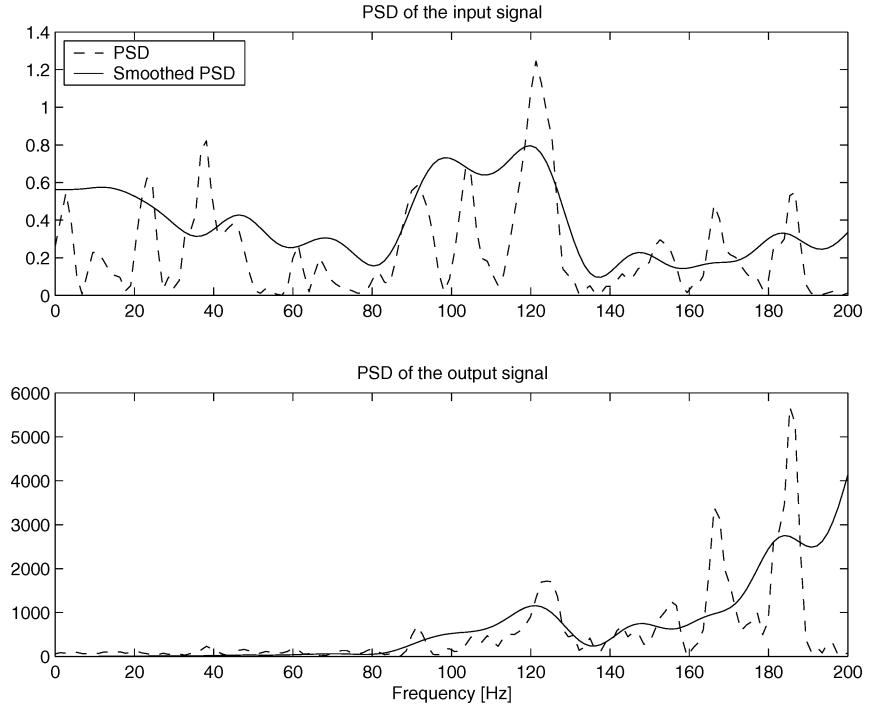

Fig. 1 Power spectral densities of the random excitation signal and the GAF response: heave mode, Mach 0.3.

Frequency-Domain GAF ROM

As a preliminary study, a ROM was identified for the GAF that develop in response to a rigid-body heave motion, at Mach number of 0.3. This case represents an attempt to perform the simplest possible identification task. The identification is of a single-input/single-output system (SISO); the aerodynamic response to the heave mode is associated only with the velocities of the prescribed motions (and not with the velocities and displacements as would be the case for the other modal motions); and the choice of low transonic Mach number ensures that the physics of the problem is linear.

The first data set consists of the response of the CFD system to a random excitation of the heave mode. The amplitude of the excitation signal was limited to $\xi = \pm 0.001$. The physical displacements at the wing surface grid points $\{u\}$ were calculated by a modal transformation $\{u\} = \{\phi_h\}\xi$, in which $\{\phi_h\}$ is the heave mode described in the wing's surface grids. The heave mode was normalized such that a modal displacement of 1 corresponds to a physical displacement of 1 in. Therefore, a modal displacement bounded between $\xi = \pm 0.001$ corresponds to a physical displacement bounded between ± 0.001 in. This way, the grid displacements and velocities are kept small, in accordance with the basic assumption of small perturbations about the steady-state flow conditions.

Figure 1 presents the PSD of the input random signal and its response, in the frequency range of 0–200 Hz. The dashed line represents the PSD of the raw data, and the full line represents the smoothed PSD that was computed by Welch's modified periodogram method, using eight nonoverlapping segments. A correlation can be observed between the excitation and the response, and the coherence function for the raw data equals to one, indicating that the signal shown in the lower plot is indeed a response to the excitation signal shown in the upper plot, and not to spurious excitation. The coherence function, which is a measure of the correlation between two signals, is defined as

$$C_{\xi F_A}(k) = \frac{|P_{\xi F_A}(k)|^2}{P_{\xi\xi} P_{F_A F_A}} \tag{17}$$

Figure 2 presents the GAF frequency response, computed from the random data set, as real and imaginary parts of the complex frequency response. The dashed line corresponds to the frequency response evaluated from PSDs of the raw data, whereas the full line was computed using the smoothed PSDs. The starts in Fig. 2 are from direct frequency analysis and serve as a reference for the GAF frequency response. The direct frequency analysis is based on a time-marching CFD analysis in which only one frequency is excited. After the transient response decays, the gain and phase shift between the output and input are evaluated, and the process is repeated for several frequencies within the frequency band of interest. Figure 2 shows a match between the ROM (based on the random data) and direct frequency analysis, indicating that the random data set is informative. The frequency response evaluated from the raw data is erratic and cannot be used, as it is, for further analyses. The frequency response based on the smoothed PSDs is a smooth function of the frequency and captures very well the system's response at the frequencies tested (the stars).

Figure 3 presents a GAF frequency response evaluated from the data set of response to FWGN input signal. The FWGN input signal was created by taking a numerically generated random time series with Gaussian distribution and filtering it to include frequencies of up to 0.1 the sampling frequency. As mentioned before, the input signal corresponds to time intervals of 0.05 nd-s, that is, sampling frequency of 20 cyc/nd-s, or approximately 22,000 Hz. Filtering the signal to 0.1 of the sampling frequency still leaves very large frequency content in the signal (Nyquist frequency of about 1100 Hz), over 10 times the highest frequency of interest.

The frequency response of Fig. 3 is smooth and captures well the system's frequency response, indicating that the FWGN signal is well suited for purpose of identification of frequency response models. Therefore, the following identification data sets of this study are all based on FWGN input signals.

This ROM identification approach was applied to the identification of GAFs of the four elastic modes of the AGARD 445.6 wing. Figure 4 presents the GAF complex transfer function corresponding to Mach 0.9 as real and imaginary parts (the full and dashed lines, respectively). The A_{ij} plot corresponds to the ith mode generalized aerodynamic force coefficient that develops in response to excitation of the jth mode, as a function of the excitation reduced frequency. The stars present the results of direct frequency analysis and serve as the reference data. The ROM matches very well the direct response. From Fig. 4 it can seem like the ROM does not capture the responses of the third mode to excitations of the first and second modes very accurately. However, the amplitudes of these responses are an order of magnitude smaller than the amplitudes of the other modes GAFs to the same excitations. Overall the

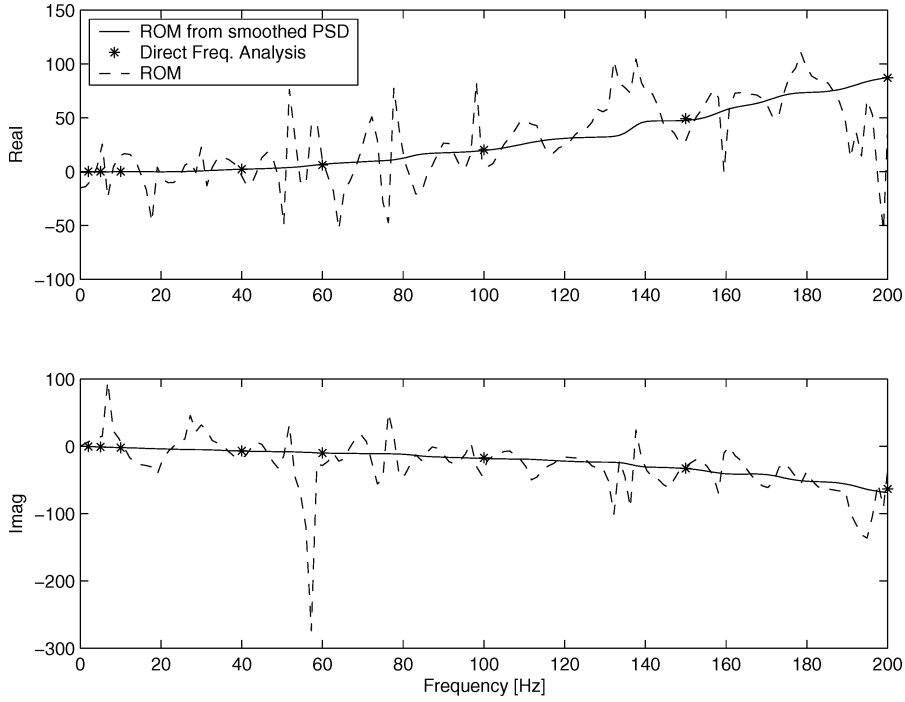

Fig. 2 Comparison of ROM and direct frequency response: heave mode, Mach 0.3, random excitation.

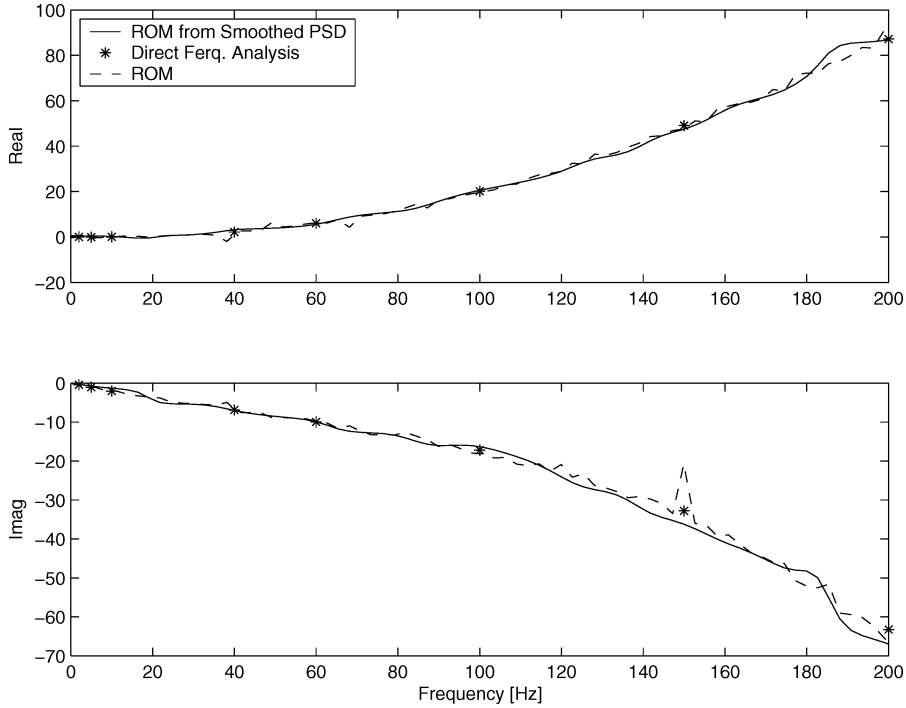

Fig. 3 Comparison of ROM and direct frequency response: heave mode, Mach 0.3, FWGN excitation.

GAF ROM seems to be a very good representative of the system's behavior.

The identification of the GAFs of Fig. 4 was based on a data set of 2^{13} points, that is, the response of the CFD to the excitation was recorded over 2^{13} time steps (CFD iterations). Reducing the data length to 2^{11} resulted in GAF matrices similar to those of Fig. 4; however, reducing the data length below 2^{11} deteriorated the quality of the GAFs. The required data length is important, especially for realistic aeroelastic analysis, in which many modes are involved. For the current case, the computational time for running CFD responses for a four mode, 500K grid points, 2^{11} time steps, one Mach number, is small, approximately 1 h on 12 MIPS R10000 250-MHz processors. For more realistic cases the computational time required for preparing the identification data can be significant.

Figure 5 compares the GAFs of the first two elastic modes to those computed by ZAERO's linear aerodynamic panel method (see Chap. 3 of Ref. 13). The resemblance of the CFD and linear aerodynamic responses point out that the case at hand is not highly linear.

The GAF ROM just identified is a nonparametric model, in which the complex transfer function is provided at a number of reduced frequencies defined by the user. An advantage of this model is that the GAF matrices can be evaluated at many reduced frequencies, without significant computational cost. Compared to the time-domain nonparametric models, such as the step/impulse response of Ref. 8,

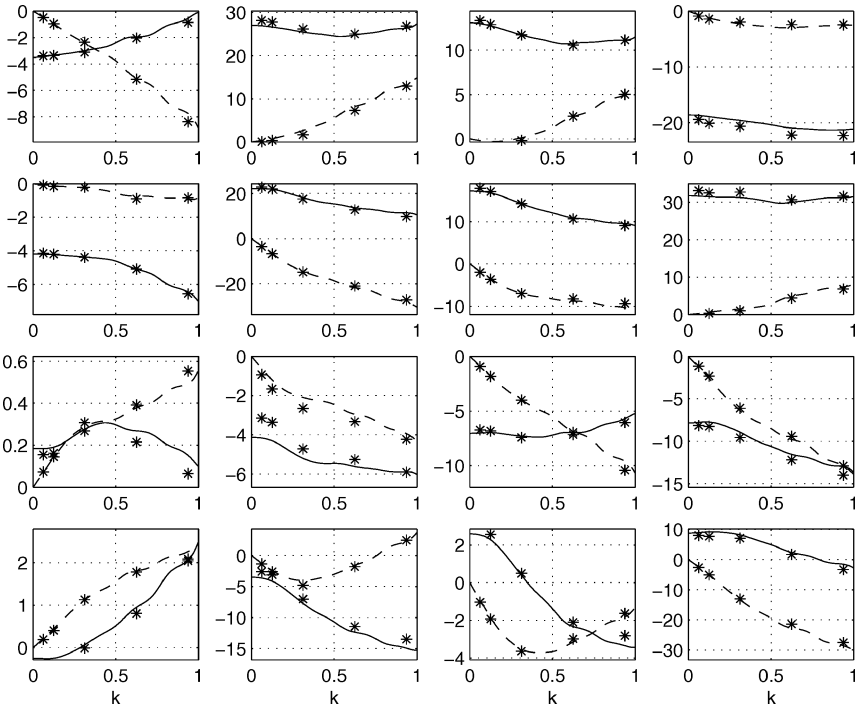

Fig. 4 GAF of the first four elastic modes: as real (——) and imaginary (– – –) parts Mach 0.90.

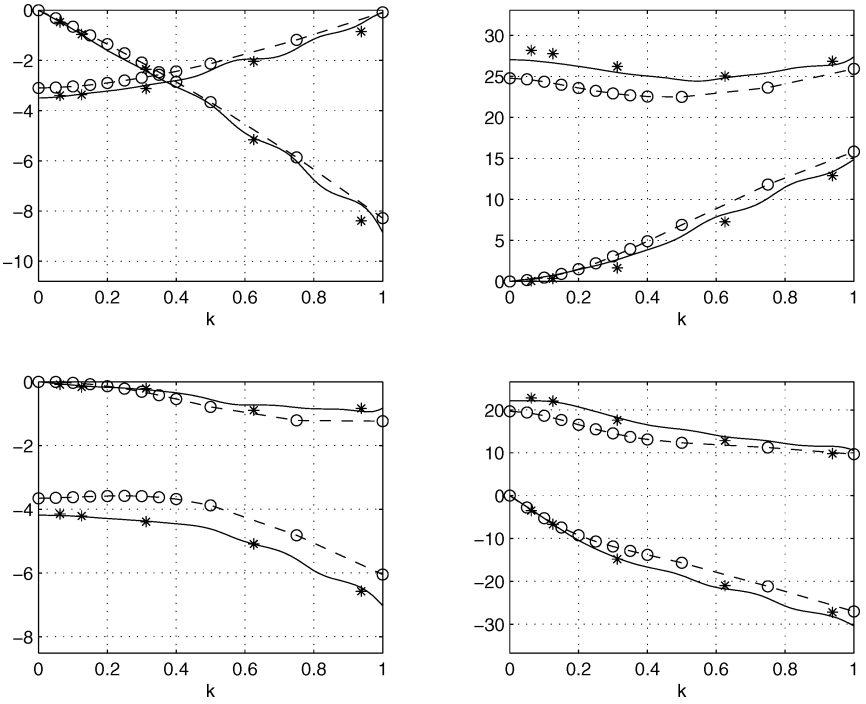

Fig. 5 Comparison of CFD-based GAFs (——) and linear GAFs (– – –) for the first two elastic modes: Mach 0.90.

where the evaluation of GAF at a single reduced frequency required applying convolution summation, this model has the advantage that the GAFs are readily available, from spectral analysis, at as many frequencies as desired. The data length is not an upper limit for the number of frequency points. If the GAFs are desired in a number of frequencies larger than the number of data points, the data are padded with zeros for the spectral analysis.

Frequency-Domain Flutter Analyses

The GAF ROM of Fig. 4 was used to evaluate the flutter characteristics of the AGARD 445.6 wing, at Mach 0.9, via a k-method flutter analysis implemented in a MATLAB routine, and via a g-method flutter analysis in ZAERO (see Chap. 7 of Ref. 13). Figure 6 shows k-method $\omega - V - g$ plot. The plot is presented in order to demonstrate the benefits of having GAFs available at many reduced frequencies (at almost no computational cost), which results in smooth $\omega - V - g$ curves and minimal need for interpolations.

Flutter characteristics from both k- and g-method analyses are summarized in Table 1, together with flutter results from wind-tunnel tests as reported by Ref. 12, and g-method results using linear aerodynamics. Flutter speed index and flutter frequency ratio are derived from normalization provided in Ref. 8. The fact that

Table 1 Flutter characteristics for the AGARD 445.6 wing, Mach 0.9

Method	Flutter speed, ft/s	Flutter frequency, r/s	Flutter speed index	Flutter frequency ratio
Wind-tunnel test	973.4	101.1	0.37	0.42
g method with linear aero.	980.8	102.6	0.37	0.43
g method with ROM	920.4	104.2	0.35	0.44
k method with ROM	935.5	106.3	0.36	0.44

wind-tunnel tests and flutter analyses using linear and nonlinear aerodynamics result in close flutter characteristics indicates that the case at hand is only mildly nonlinear, and therefore it is somewhat surprising that the CFD results deviate from linear results as much as they do. It is possible that this deviation can be attributed to the ROM. An indication for this is that latter flutter results, obtained with a different time-domain ROM, as shown on Fig. 15, are much closer to the wind-tunnel tests. Not only the ROM but also the flutter method affects the flutter results. This is seen from Table 1 in comparing the flutter characteristics obtained by the g and k methods

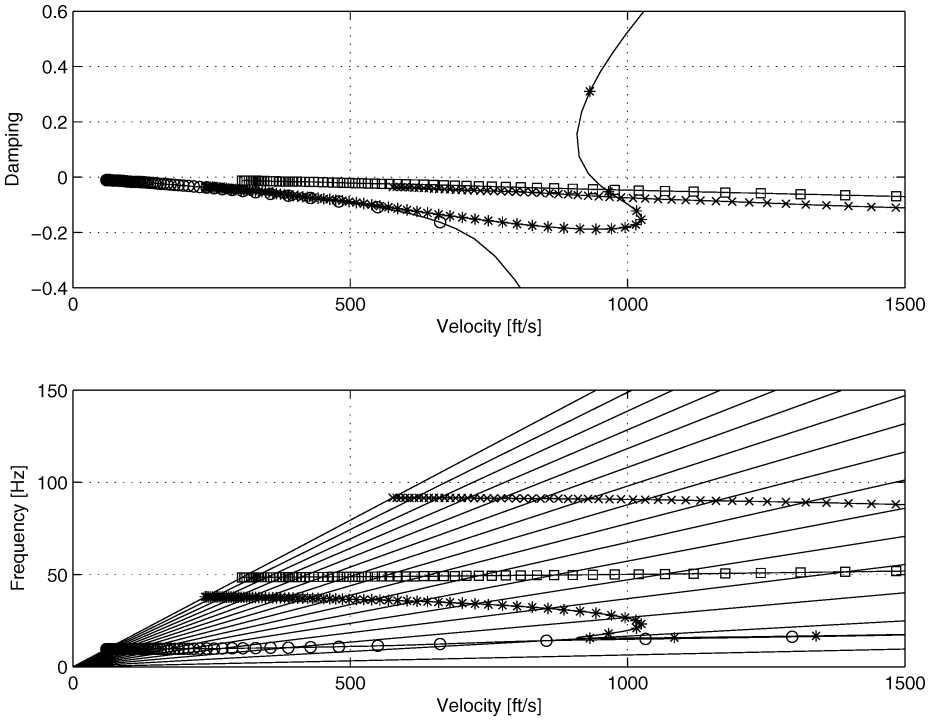

Fig. 6 ωVg plot from k-method flutter analysis using the GAF ROM: Mach 0.9.

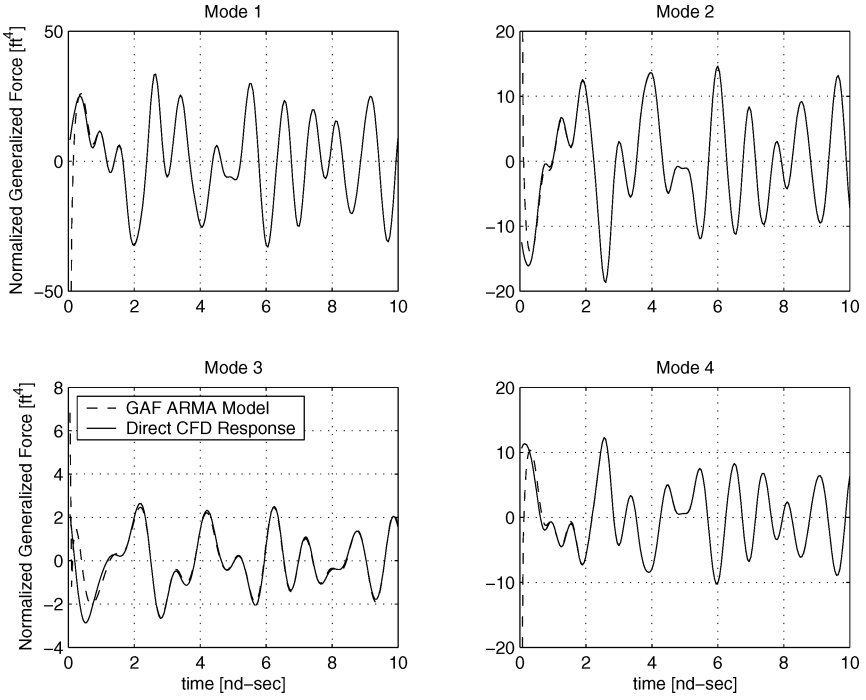

Fig. 7 Comparison of ARMA model simulated response and measured CFD response to WGN excitation of the first elastic mode: Mach 0.9.

using the same ROM. Finally it is possible that it is the CFD method and (or) grid that contribute to the discrepancies of Table 1. However, this study intentionally stays away from general issues of CFD/grid adequacy. The ROM method can be practiced with any CFD available and with typical-size grids.

Time-Domain GAF ARMA and State-Space Models

The FWGN data set was used for the identification of time-domain GAF ARMA and state-space models. For the ARMA model, the identification was based on as little as 128 data points, whereas the rest of the data ($2^{13}-128$ points) served for model validation. The model size that was found to best represent the identification data is $na=4$, $nb=8$. The next two figures present results of identification of responses to excitation of the first elastic mode, Mach 0.9. Figure 7 presents response time histories, comparing the simulated model output to measured CFD response. Only a small part of the validation data is showing. The GAF ARMA model was also validated using responses to harmonic sinusoidal excitations of various frequencies, in the frequency range of interest, and was found to be very good representative of the system. Figure 8 shows a comparison of the time histories of GAF in response to sinusoidal excitation of the first mode in frequency of 50 Hz, computed using the GAF ARMA model and directly in a CFD run. As was the case for the frequency-domain modeling, the GAF model for the response of the third mode to excitation of the first mode is less accurate than the others, but its amplitude is small compared to the other responses.

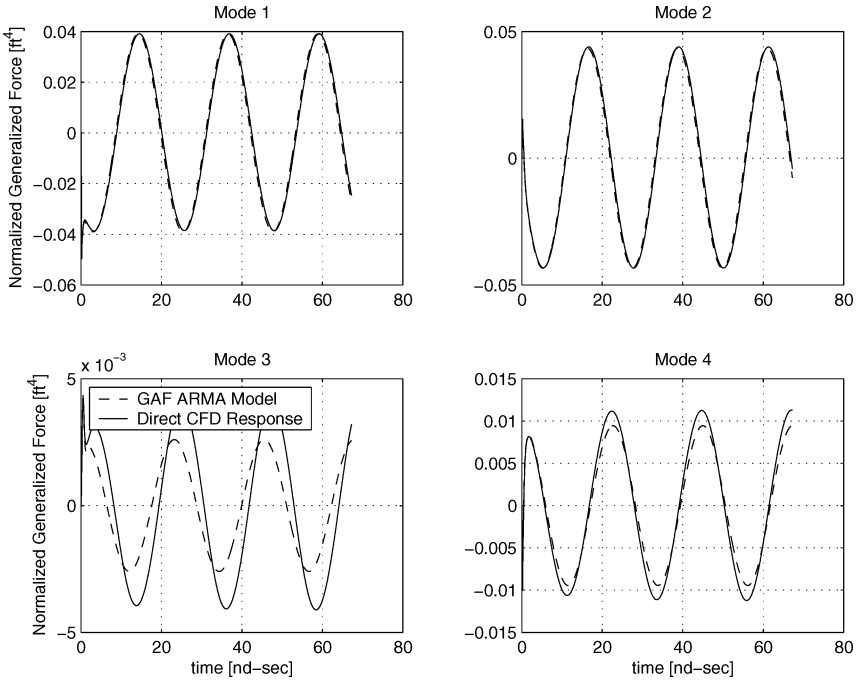

Fig. 8 Comparison of ARMA model simulated response and measured CFD response to sinusoidal excitation of the first elastic mode: Frequency = 50 Hz, and Mach 0.9.

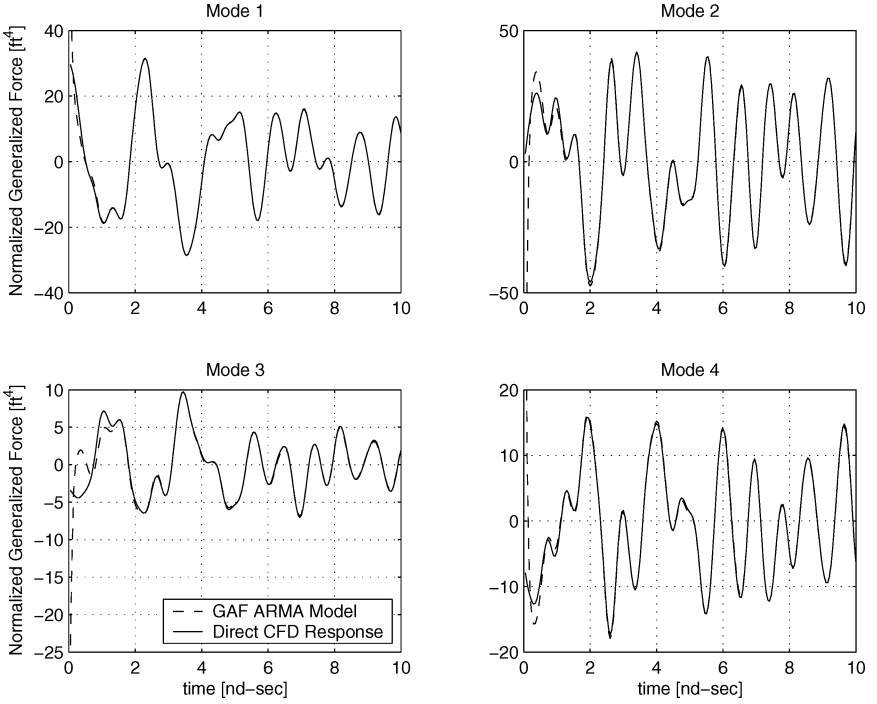

Fig. 9 Comparison of ARMA model simulated response and measured CFD response to FWGN excitation of the second elastic mode: Mach 0.9.

The identification process was repeated for modes 2–4, using the same model orders. Figures 9–11 present time histories of responses to the validation data, comparing the simulated model output to measured CFD responses, all showing excellent agreement.

For the identification of a four-input/four-output state-space model, the responses from the four CFD runs were concatenated such that the validation data are now of size $4N$ by 4, where N is the length of each data set (number of samples). It was necessary to identify a four-input/four-output ROM rather than identify a separate ROM for each mode because the latter would result in four different state matrices. The state-space model is of order 12 and was evaluated based on 2048 samples of the identification data. It was found that in order to accurately identify the four-by-four model, longer data sets are necessary (2048 samples vs 128 in the one-by-four case).

Figure 12 presents time histories of the response to FWGN excitation of the first elastic mode, at Mach 0.9, comparing the state-space four-by-four model simulated response and measured CFD response.

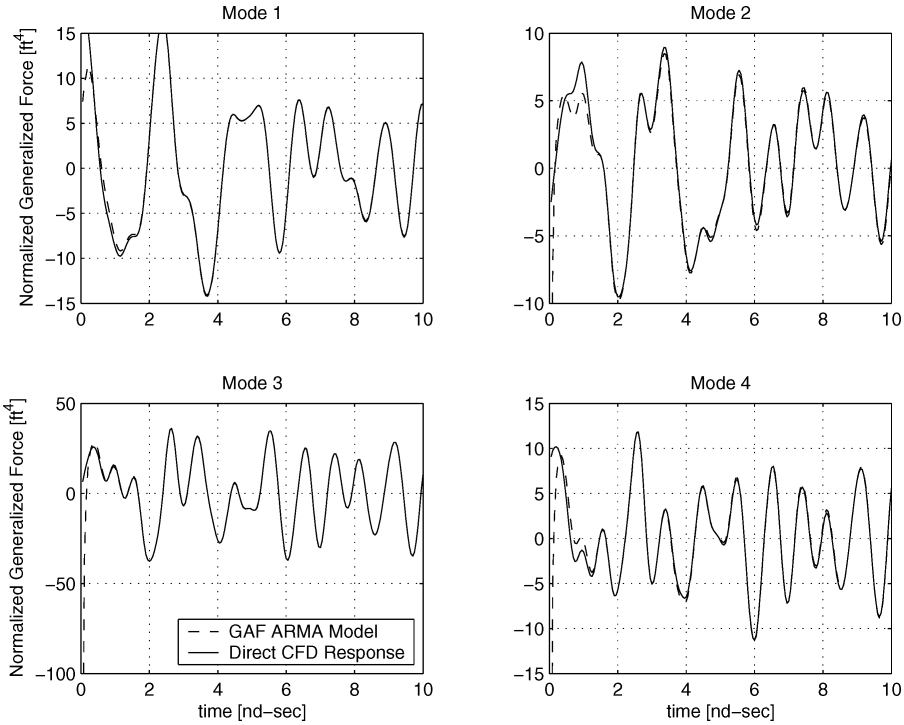

Fig. 10 Comparison of ARMA model simulated response and measured CFD response to FWGN excitation of the third elastic mode: Mach 0.9.

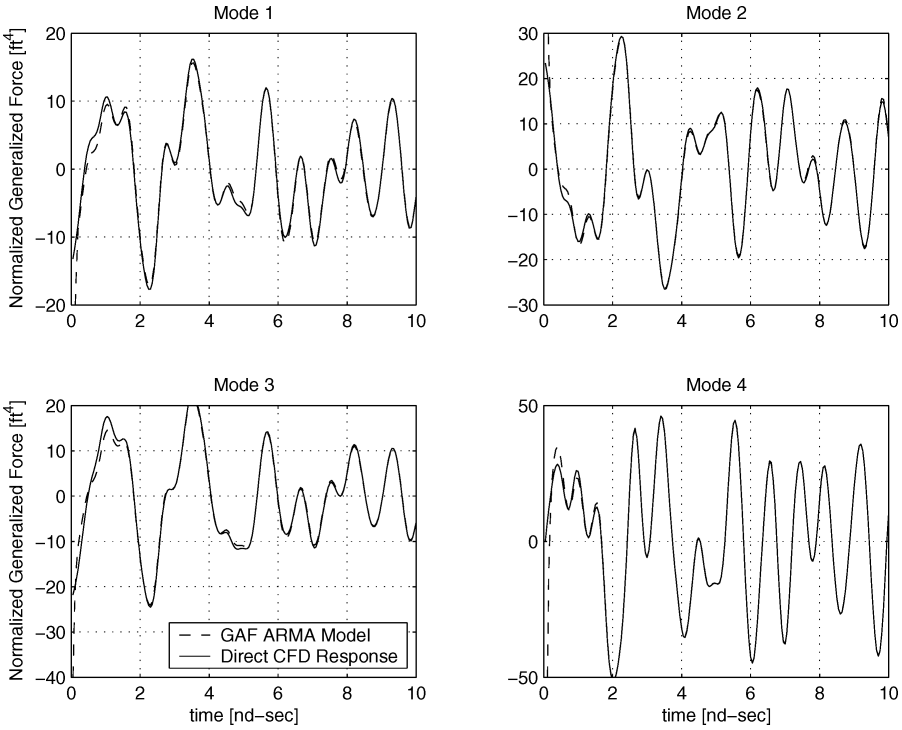

Fig. 11 Comparison of ARMA model simulated response and measured CFD response to FWGN excitation of the fourth elastic mode: Mach 0.9.

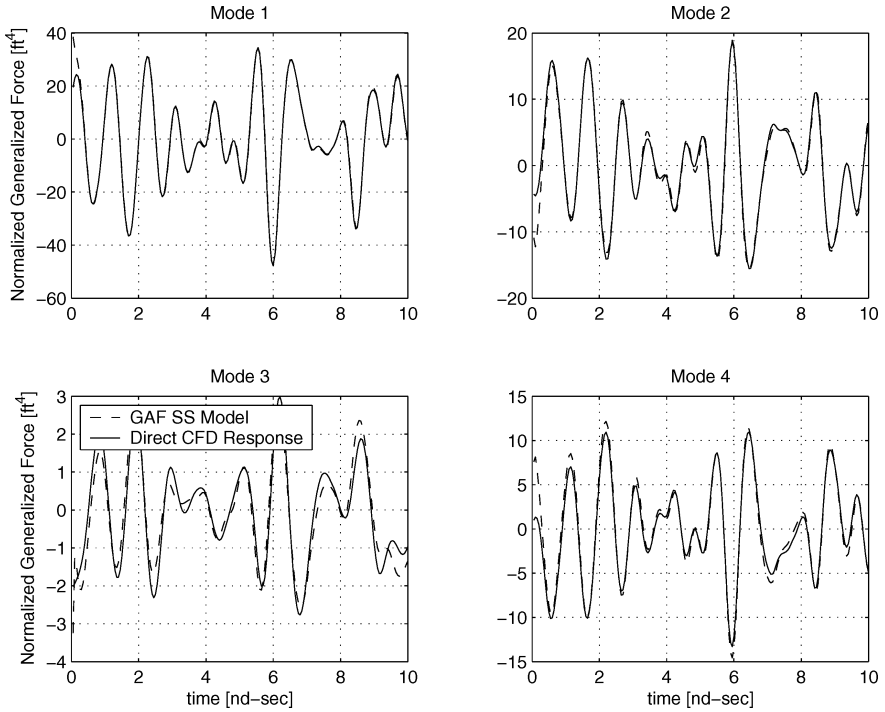

Fig. 12 Comparison of state-space model simulated response and measured CFD response to FWGN excitation of the first elastic mode: Mach 0.9.

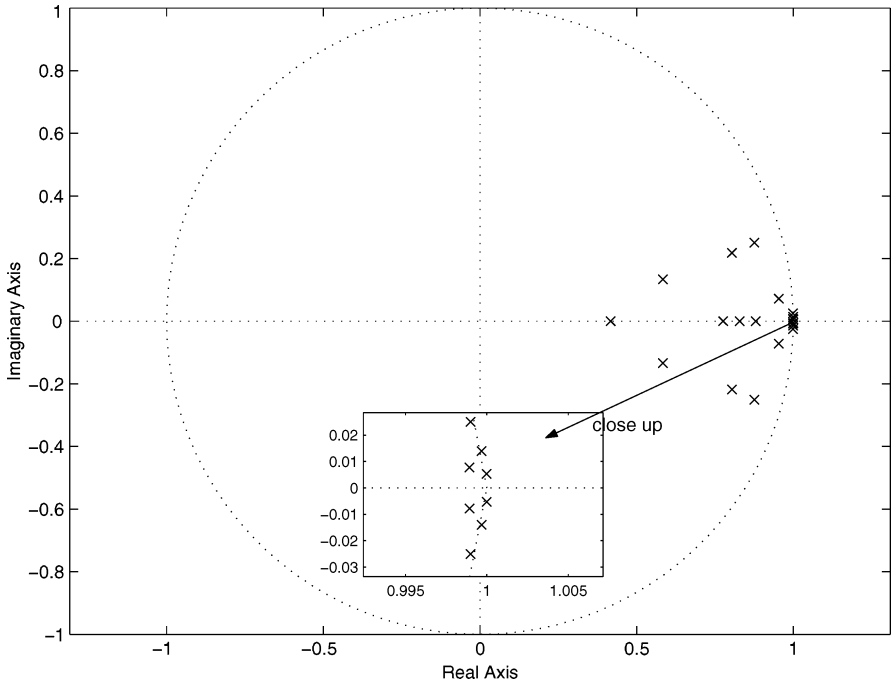

Fig. 13 Pole map of the aeroelastic system at flutter dynamic pressure.

The accuracy of the three models, the frequency domain, ARMA, and state-space, is evaluated based on their ability to reproduce the validation data (which is different from the data that were used for training). A fit parameter was defined as

$$\eta = \left(1 - \sqrt{\frac{\sum_{i=1}^{N}\left(F_{A_i} - \hat{F}_{A_i}\right)^2}{\sum_{i=1}^{N} \boldsymbol{F}_{A_i}^2}}\right) \tag{18}$$

where F_A and $\hat{F}_A$ are the vectors of measured and simulated aerodynamic force, respectively. A fit parameter of 1 indicates a perfect fit between the simulated and measured values. Table 2 presents comparison of the fit parameters of the three models. These fit parameters were evaluated based on some validation data that consist of the time histories of all generalized forces in response to 1) FWGN excitation of the first elastic mode and 2) 10- and 50-Hz sinusoidal excitation of the first elastic mode. From Table 2 it is seen that, based on the fit parameter of Eq. (18), the various models are all good, and the choice of model will thus be a function of the application for which the model is needed. With regards to ease of implementation, all models are very easy to implement, using MATLAB built-in functions and toolboxes. The advantage of time-domain models over frequency-domain models is that they require relatively short data sets for accurate identification.

Table 2 Comparison of models based on a fit parameter

Model	Filtered WGN	Harmonic 10 Hz	Harmonic 50 Hz
Freq. resp.	——	——	0.9243
ARMA	0.9121	0.9487	0.9069
State space 1×4	0.9136	0.9479	0.9099
State space 4×4	0.9634	0.7021	0.7460

Time-Domain Flutter Analysis

The aerodynamic state-space model was combined with the structural discrete-time state-space model according to Eq. (16). The dynamic pressure was varied, and the flutter dynamic pressure was found by examining the location of the roots of the discrete aeroelastic system. Figure 13 presents the pole map of the aeroelastic system at a dynamic pressure of 92 lb/ft^2, at which the first root crosses

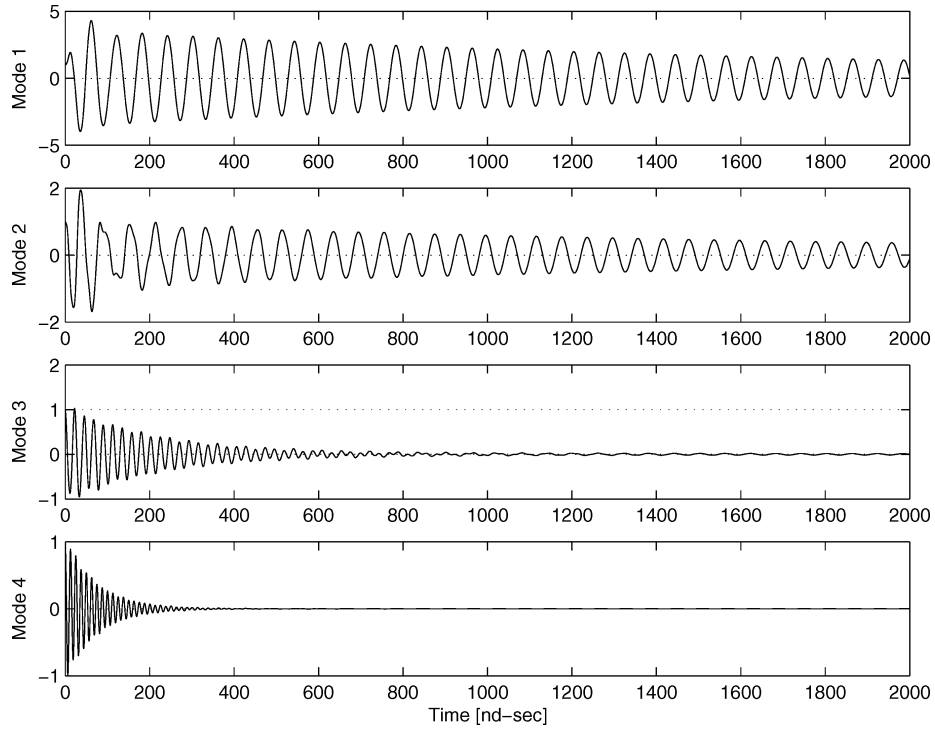

Fig. 14 Response of the aeroelastic system to initial conditions at $V = 970$ ft/s, below flutter speed.

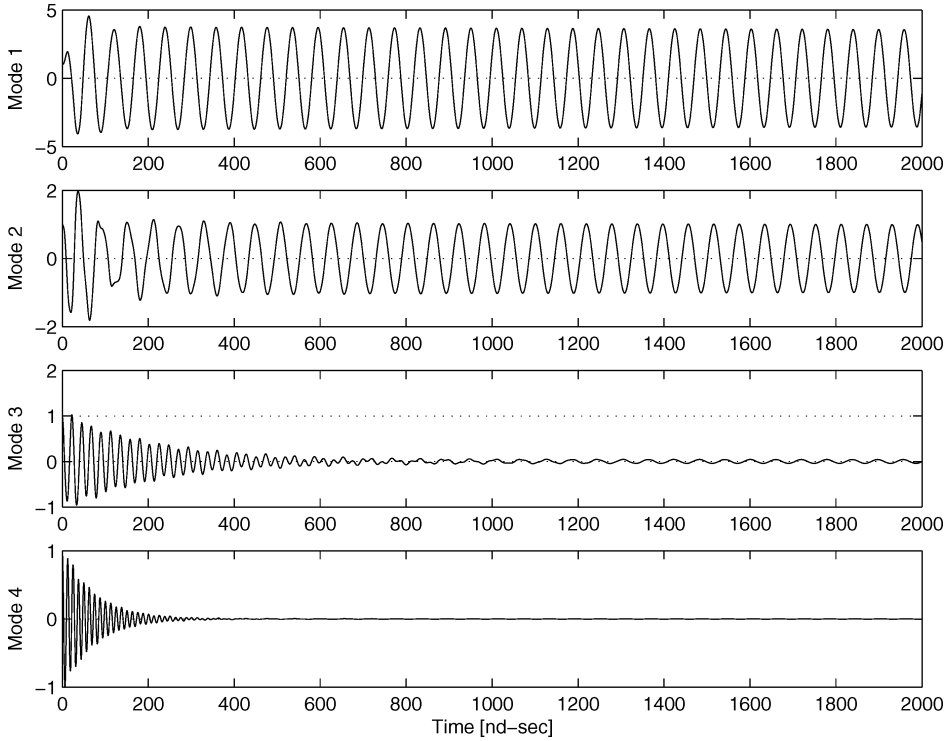

Fig. 15 Response of the aeroelastic system to initial conditions at the flutter speed: $V = 976$ ft/s.

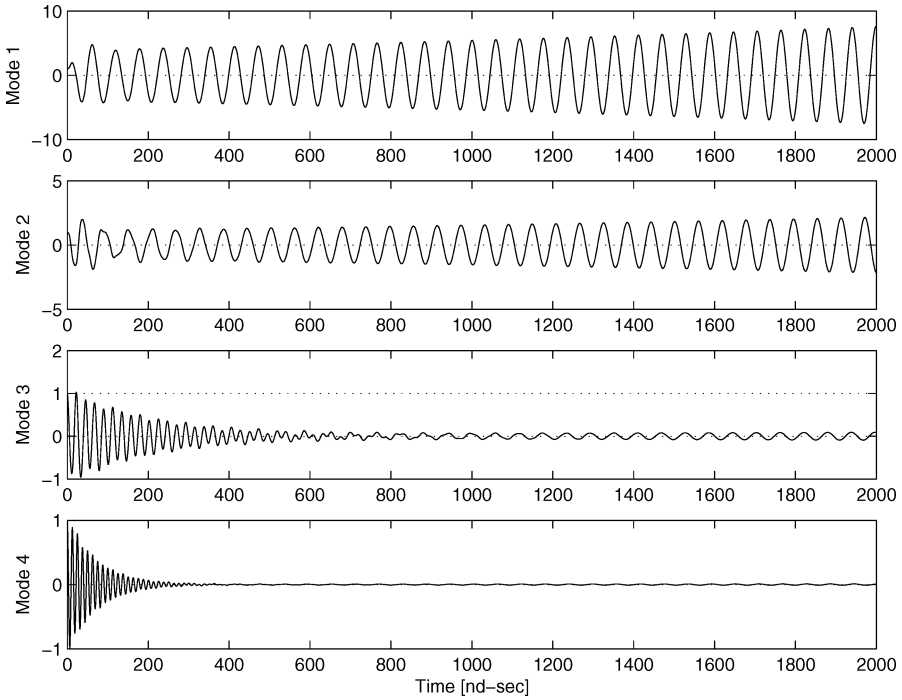

Fig. 16 Response of the aeroelastic system to initial conditions at $V = 980$ ft/s, above flutter speed.

outside of the unit circle, indicating that the system is becoming unstable. This crossover point corresponds to a flutter velocity of $V_f = 976$ ft/s and to flutter frequency of $\omega_f = 110$ rad/s. Figures 14, 15, and 16 present time histories of responses to initial conditions of the aeroelastic system at velocities below, at, and above the flutter velocity. These simulations execute in only a fraction of a second, offering significant advantage over the very long execution time of the full CFD-coupled aeroelastic simulation.

Summary

The paper presented three system-identification methods that were used for the identification of unsteady aerodynamics linearized reduced-order models (ROMs). A filtered white-Gaussian-noise (FWGN) signal that was used for identification was found to be applicable within the computational-fluid-dynamics (CFD) code, and resulted in very informative data sets. Three models were identified: a frequency-domain model, a time-domain ARMA model, and a discrete-time state-space model. The models were validated based on their ability to reproduce CFD responses to various excitations, including a FWGN excitation and sinusoidal excitations of various frequencies and were found to be very accurate. A fit parameter, which is a measure of the model's ability to reproduce CFD outputs, was computed and was found to be close to a value of one for all models, indicating high model accuracy. Frequency-domain ROMs were used in flutter analyses based on the k and g methods. It was demonstrated that with the spectral analysis identification approach GAF matrices could be evaluated at many reduced frequency values requiring only little computational cost. Time-domain ARMA and state-space aerodynamic models were evaluated directly from the time-domain CFD responses, and a state-space model of the aeroelastic system was used for evaluation of the flutter boundaries via root mapping. The estimated flutter boundaries were close to flutter boundaries computed using CFD and linear aerodynamics and to those from wind-tunnel tests. The state-space model provided a means for very rapid simulations of the aeroelastic system compared to the full time-stepping CFD aeroelastic analysis, and can serve in future work for CFD-based aeroservoelastic analyses.

The ROM approaches presented in this study should be further tested, possibly with more complex configurations and at clearer nonlinear flow conditions. Based on the test case of this study, these methods hold significant potential for producing CFD-based time- and frequency-domain models. They can possibly eliminate the need for rational function approximations in generating time-domain unsteady aerodynamic models, and likely serve for modeling transonic unsteady aerodynamics.

References

[1] Yurkovitch, R., Liu, D. D., and Chen, P. C., "The State-of-the-Art of Unsteady Aerodynamics for High Performance Aircraft," *CEAS International Forum on Aeroelasticity and Structural Dynamics*, AIAA Paper 2001-0428, Vol. 1, 2001, pp. 47–68.

[2] Dowell, E. H., "Eigen-Mode Analysis in Unsteady Aerodynamics: Reduced-Order Models," *AIAA Journal*, Vol. 34, No. 8, 1996, pp. 1578–1583; also AIAA Paper 0001-1452, April 1995.

[3] Silva, W., Beran, P., Cesnik, C., Guendel, R., Kurdila, A., Prazenica, R., Librescu, L., Marzocca, P., and Raveh, D., "Reduced-Order Modeling: Cooperative Research and Development at the NASA Langley Research Center," *CEAS International Forum on Aeroelasticity and Structural Dynamics*, Asociacion de Ingenieros Aeronauticos de Espana, Vol. 2, Madrid, Spain, 2001, pp. 159–174.

[4] Beran, P., and Silva, W., "Reduced-Order Modeling—New Approaches for Computational Physics," AIAA Paper 2001-0853, Jan. 2001.

[5] Ballhaus, W. F., and Goorjian, P. M., "Computation of Unsteady Transonic Flows by Indicial Methods," *AIAA Journal*, Vol. 16, No. 2, 1978, pp. 117–124.

[6] Lee-Rausch, E. M., and Batina, J. T., "Wing Flutter Boundary Prediction Using Unsteady Euler Aerodynamic Method," *Journal of Aircraft*, Vol. 32, No. 2, 1995, pp. 416–422.

[7] Silva, W. A., "Discrete-Time Linear and Nonlinear Aerodynamic Impulse Responses for Efficient CFD Analysis," Ph.D. Dissertation, Faculty of the Dept. of Applied Sciences, College of William and Mary, Williamsburg, VA, Oct. 1997.

[8] Raveh, D., Levy, Y., and Karpel, M., "Efficient Aeroelastic Analysis Using Computational Unsteady Aerodynamics," *Journal of Aircraft*, Vol. 38, No. 3, 2001, pp. 547–556.

[9] Cowan, T. J., Arena, A. S., Jr., and Gupta, K. K., "Accelerating Computational Fluid Dynamics Based Aeroelastic Predictions Using System Identification," *Journal of Aircraft*, Vol. 38, No. 1, 2001, pp. 81–87.

[10] Cowan, T. J., Arena, A. S., Jr., and Gupta, K. K., "Development of a Discrete-Time Aerodynamic Model for CFD-Based Aeroelastic Analysis," AIAA Paper 99-0765, Jan. 1999.

[11] Silva, W., and Bartels, R., "Development of Reduced-Order Models for Aeroelastic Analysis and Flutter Prediction Using the CFL3Dv6.0 Code," AIAA, 43rd Structures, Structural Dynamics and Materials Conf., AIAA Paper 2002-1596, April 2002.

[12]Yates, E. C., Jr., "AGARD Standard Aeroelastic Configurations for Dynamic Response. Candidate Configuration I.—Wing 445.6," NASA TM-100492, 1987.
[13]"ZAERO Theoretical Manual," Ver. 6.0, Zona Technology, Inc., Scottsdale, AZ, May 2002.
[14]Welch, P. D., "The Use of Fast Fourier Transform for the Estimation of Power Spectra: A Method Based on Time Averaging Over Short, Modified Periodograms," *IEEE Transactions on Audio Electroacoustics*, Vol. AU-15, June 1967, pp. 70–73.
[15]"MATLAB® Signal Processing Toolbox User's Guide," Ver. 6.0, The MathWorks, Inc., Natick, MA, July 2002.
[16]Ljung, L., *System Identification, Theory for the User*, 2nd ed., Prentice–Hall, Upper Saddle River, NJ, 1999, Chap. 7.3, pp. 203–211.
[17]"MATLAB System Identification Toolbox User's Guide," Ver. 5.0, The MathWorks, Inc., Natick, MA, April 2001.
[18]Franklin, G. F., and Powell, D., *Digital Control of Dynamic Systems*, 1st ed., Addison Wesley Longman, Reading, MA, 1980, Chap. 6, pp. 131–139.
[19]Levy, Y., "Numerical Simulation of Dynamically Deforming Aircraft Configurations Using Overset Grids," *Journal of Aircraft*, Vol. 38, No. 2, 2001, pp. 349–354.
[20]Raveh, D., Levy, Y., and Karpel, M., "Structural Optimization Using Computational Aerodynamics," *AIAA Journal*, Vol. 38, No. 10, 2000, pp. 1974–1982.